

MODELLING OF PARTICULATE FOULING ON HEAT EXCHANGER SURFACES: INFLUENCE OF BUBBLES ON IRON OXIDE DEPOSITION.

D.H. Lister and F.C. Cussac

Department of Chemical Engineering, University of New Brunswick, PO Box 4400, Fredericton, NB, Canada, E3B 5A3
dlister@unb.ca
francois.cussac@unb.ca

ABSTRACT

Studies of iron oxide deposition on Alloy-800 heat-exchanger tubes have been part of a continuing research program at the University of New Brunswick; the present work formulates mechanisms for the effect of bubbles on deposition in water under boiling conditions.

To supplement results from earlier deposition experiments in a fouling loop at UNB, measurements of bubble frequency and departure diameter as a function of heat flux were performed. High-speed movies of bubbling air/water systems indicated that a pumping action moved particles from adjacent areas at the surface to bubble nucleation sites.

To explain the observations, the model considers deposition and concomitant removal. Deposition includes microlayer evaporation and filtration through the porous deposit. The deposit is sparse in the first stage, when the dominant process is microlayer evaporation including particle trapping and pumping, creating spots of deposit. Filtration becomes more important as the deposit thickens to a stage when microlayer evaporation becomes negligible. Chimney effects then control. Turbulence due to detaching and collapsing bubbles affects removal. In sub-cooled boiling, collapsing bubbles generate enough turbulence to maintain much of the deposit labile while in bulk boiling bubble detachment from the nucleation site is dominant and a smaller portion of the deposit is labile and subject to removal. Model predictions are presented and shown to agree quite well with experimental data.

INTRODUCTION

A program is continuing at the University of New Brunswick to investigate fouling of Alloy-800 heat exchanger tubes by iron oxides particles. The objective is to understand and ultimately control the fouling of cooling circuits such as the secondary system in nuclear power plants.

Mathematical models for particulate fouling have been created by previous workers. Kern and Seaton (1959) were the first to describe net deposition as the competition between a deposition flux and a removal flux. Later on, Asakura (1978) studied the effect of microlayer evaporation and dry-out of the liquid underneath nucleating bubbles in the sub-cooled boiling regime. In recent years, consolidation has been proposed as a major mechanism in

fouling. Turner and Klimas (2001) derived a consolidation model based on a two-layer deposit with a labile portion and a consolidated portion. It assumed that the portions interacted with each other, leading to the model expression.

At UNB, parameters such as time, pH, particle concentration and heat transfer regime have been experimentally studied. Also, radiotracing experiments were performed by Basset (2000) and Cossaboom (2005), in which irradiated particles were deposited on heated test sections. The activity on a heater tube was monitored on-line in order to study the evolution of the deposit. After a long period, about 300 hours, non-irradiated particles were introduced instead of irradiated ones. The activity decreased significantly, suggesting removal of the previously-deposited particles even as deposition of the new particles continued unseen. One experiment was conducted under sub-cooled boiling while the second one was under bulk boiling conditions. The results show significant differences, revealing an effect of the boiling intensity on deposition.

Basset, who studied radioactive magnetite deposition under sub-cooled boiling, found good agreement of his experimental data with a simple first-order Kern and Seaton model. During his removal or exchange period, the activity seemed to approach zero. Later, Cossaboom, in a similar experiment with nickel ferrite under bulk boiling, could not fit either the straightforward Kern and Seaton or Turner and Klimas models to her results. Deposition was almost linear and release/exchange affected only about a third of the deposit.

The objective of the present work is to describe the main mechanisms occurring during boiling and to determine how bubbles influence the deposition of iron oxide particles. Deposition, removal and consolidation of the deposit are included in the new model. Filtration through the porous layer already deposited is responsible for the creation of the chimney effect and is also included. Model predictions are compared to experimental data and in particular to the two radiotracing experiments described above.

MODEL DESCRIPTION

The growth of bubbles on heat transfer surfaces has been extensively studied. In the present work and for simplicity in writing the model, we assume that each nucleation site creates bubbles and is not disturbed by

adjacent sites. One nucleation at one site is studied first, and then the global deposition flux is calculated using active nucleation site density and nucleation frequency over a unit area. The pH of the liquid is such that transport effects rather than surface effects control.

Deposition

The evaporation at the “centre” spot created during bubble growth underneath the centre of the bubble, and the water coming in at detachment to fill this spot, are important mechanisms for particulate deposition. A typical nucleating bubble at a nucleation site is shown on Fig. 1.

The volume V_1 within the microlayer is calculated by assuming that all the heat coming from the surface within the radius R_b is absorbed by its evaporation. The volume V_2 is the volume of the microlayer evaporated at the centre spot. Finally, V_t is the hypothetical volume that would be occupied by a monolayer of particles around the bubble. This volume will be called the “skin” of the bubble. It is used to represent the trapping mechanism and the region of influence of the bubble surface interacting with the particles in the liquid.

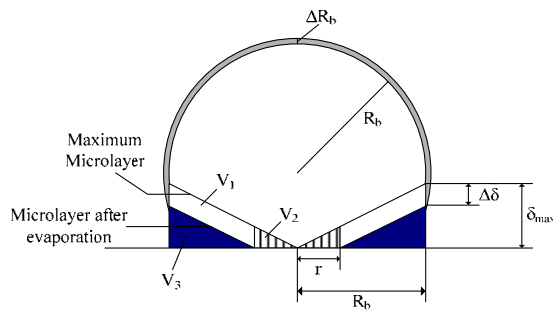


Fig. 1 Growth of a bubble at a nucleation site

Microlayer evaporation was modelled by Asakura (1978) as the ratio of the volumes V_2 over V_1 and is written as follows:

$$K = \left(\frac{4}{3}\right)^3 \left(\frac{R_b \rho_v}{\delta_{\max} \rho_w}\right) \quad (1)$$

This deposition constant K (dimensionless) can be calculated at any time, knowing the bubble growth and the growth time. R_b is the bubble radius and δ_{\max} is calculated using the relation given by Torigai (1966)

The trapping of particles is controlled by surface interactions between the growing bubble and the particles in the immediate surroundings. The concentration caused by particles trapped by the “skin” of the bubble is calculated as the concentration around the bubble (assumed to be the average of that at the wall, C_w , and that in the bulk, C_b)

multiplied by the ratio between the volume of the “skin” V_t and the volume evaporated V_1 :

$$C_{\text{trapped}} = \left(\frac{C_w + C_b}{2}\right) \zeta \int_0^t \frac{V_t}{V_1} dt \quad (2)$$

where ζ is a parameter ($0 < \zeta < 1$) representing the proportion of trapped particles that deposit. Therefore, the number of trapped particles increases as the bubble grows. It is important to notice that the parameter ζ is quite low, indicated by model fitting to be around 0.04.

The pumping action, described in the Experimental Section, is modelled as the ratio of the volume of evaporated liquid to that of the maximum microlayer multiplied by the wall concentration. It is caused by the alternating outflow of liquid during bubble growth followed by the rapid inflow at detachment. It leads to an accumulation of particles at the nucleation site. This is written as follows:

$$C_{\text{pumped}} = C_w \left(1 + \frac{V_3}{V_1 + V_2 + V_3}\right) \quad (3)$$

The complete expression for deposition at one nucleation site is then given by:

$$\varphi_{\text{nucl}} = \frac{q}{L} K (C_{\text{trapped}} + C_{\text{pumped}}) \frac{A_{\text{site}}}{f} \quad (4)$$

where q is the surface heat flux, L is the latent heat of vaporisation, f is the bubble frequency and A_{site} is the average surface area of one nucleation site, within the radius R_b .

This deposition flux is valid under both sub-cooled boiling and bulk boiling. As the surface changes because of the quantity of particles deposited, the microlayer is disturbed and as a consequence, another mechanism is included.

Iron oxide deposits are porous and allow water to percolate inside the small capillaries. When the liquid enters the capillaries, particles are filtered out and deposit on top of the deposit, increasing its thickness. However, the effect is negligible in the first stages when a deposit ring is forming around a nucleation site, since the deposit is not thick enough to allow for high filtration. The process leads to the chimney effect. To model filtration at the nucleation site, we assume that the particles depositing due to filtration are there in the liquid percolating through the porous deposit. This latter quantity is equal to the volume inside the ring of deposit, which later becomes the chimney. It can be written as:

$$V_{\text{filt}} = h \pi \left(\frac{R_b}{3} \right)^2 \quad (5)$$

where h is the thickness of the ring deposited at a time t . It can be related to the mass of iron oxide deposited on each spot, m_{spot} , as follows:

$$h = \frac{m_{\text{spot}}}{\rho_p A_{\text{site}}} = \frac{9 m_{\text{spot}}}{8 \rho_p \pi R_b^2} \quad (6)$$

When h is incorporated in the equation of the volume V_{filt} and multiplied by the wall concentration, we get the deposition by filtration per nucleation site for one nucleation:

$$\Phi_{\text{filt}} = C_w \frac{m_{\text{spot}}}{8 \rho_p} \quad (7)$$

On top of microlayer evaporation, pumping and filtration, diffusion and thermophoresis have some influence on deposition. Their impact is more noticeable on the parts of the surface with no active nucleation sites, but it also affects deposition at the nucleation sites.

The diffusion coefficient, K_{diff} , is based on the Levich model (1962) with an empirical boiling parameter BR defined by McCrea (2001).

$$K_{\text{diff}} = (1 + \text{BR}) 0.8 \frac{u^*}{\text{Sc}^{3/4}} \quad (8)$$

where u^* is the friction velocity and Sc is the Schmidt number. BR is used to account for the enhanced deposition due to boiling and is defined as follows:

$$\text{BR} = \frac{q}{L} \frac{(T_{\text{film}} - T_{\text{sat}})}{T_{\text{sat}}} \frac{a}{R_b} \quad (9)$$

where a is a constant fitted to adjust the value of BR to between 0 and 1. In our case, $a=0.05$.

The deposition flux by diffusion is now written:

$$\Phi_{\text{diff}} = (C_b - C_w) K_{\text{diff}} \quad (10)$$

At the nucleation sites, during the bubble growth, the wall concentration is higher than the bulk concentration. This will promote diffusion back to the bulk. Nevertheless, it is assumed that diffusion towards the wall in the inside of the rings of deposit occurs between the detachment of a

bubble and the formation of the next one. The driving force then becomes the difference between the bulk and the wall concentrations

The thermophoresis effect is calculated from the model of McNab and Meisen (1973):

$$K_{\text{th}} = 0.26 \frac{1}{2\lambda_w + \lambda_p} \frac{v_w}{T_{\text{sat}}} q \quad (11)$$

A hot wall will tend to repel particles and therefore this mechanism is represented as a constraint to deposition rather than a removal mechanism. The flux of particles repelled from the wall by thermophoresis can be written as:

$$\Phi_{\text{th}} = C_w K_{\text{th}} \quad (12)$$

It is important to notice that since the bubble-affected mechanisms operate for one nucleation at one nucleation site, the diffusion and thermophoresis fluxes have to be changed to corresponding units (see Eq. (14)).

Deposition outside of the nucleation sites is observed to be negligible for the first stages. A thick deposit on the full surface takes much longer time to appear in low pressure and low flow rate conditions when deposition first occurs in the form of spots and rings at nucleation sites. Thus, the net deposition flux is defined as follows:

$$\Phi_d = N_a f (\Phi_{\text{boil}} + \Phi_{\text{wait}}) \quad (13)$$

Here N_a is the active nucleation site density, and Φ_{boil} is the net deposition flux due to the bubble from its birth to detachment, at one nucleation site, during one nucleation, written:

$$\Phi_{\text{boil}} = \Phi_{\text{nucl}} + \Phi_{\text{filt}} + (\Phi_{\text{diff}} - \Phi_{\text{th}}) t_g A_{\text{site}} \quad (14)$$

where t_g is the growth time of one nucleation. Φ_{wait} is the deposition flux for the waiting period between bubble detachment and nucleation of the next one, where only diffusion, thermophoresis and filtration due to pumping have an effect on deposition. It is defined as:

$$\Phi_{\text{wait}} = (\Phi_{\text{diff}} - \Phi_{\text{th}}) t_w A_{\text{site}} + \Phi_{\text{filt}} \quad (15)$$

where t_w is the waiting time period.

Removal / Exchange

It was observed that removal behaves differently under sub-cooled and bulk boiling conditions. It affects more of the deposit for sub-cooled boiling, as observed by Basset (2000), but the first-order removal constant is lower than

that for bulk boiling. It is suggested that when a bubble collapses, it creates a certain amount of turbulence in the viscous sub-layer and disturbs the flow in the deposit vicinity. Under sub-cooled boiling conditions, the bubbles collapse close to the surface and the outer layers of deposit are permanently maintained in a labile and removable state. However, under bulk boiling conditions, bubbles collapse further away from the surface if at all and the turbulence effect is less on the deposit. Cossaboom (2005) experimentally observed that only a third of the deposit was labile and subject to removal/exchange under bulk boiling conditions. Mechanistically, this is expressed as follows. For sub-cooled boiling, the main turbulence parameter comes from the collapsing bubbles very close to the surface, whereas for bulk boiling, the detaching bubbles have the major influence. Diffusion from the deposit is included in both boiling regimes. To distinguish removal/exchange in different boiling regimes, we treat them separately in the present study, though it is likely that a smooth transition would occur in reality as sub-cooled changed to bulk boiling, through a change in pressure, for example.

The effect of the collapsing bubbles on the deposit can be represented by the intensity of the collapsing bubble (Brennen, 1995) defined as:

$$I \approx a \rho_w V \frac{R_{bc}^{3/2}}{d_s} \quad (16)$$

where a is a constant (with units allowing I to be in the units of %), V is the flow velocity in the bulk, R_{bc} is the maximum radius of the bubble just before collapsing, and d_s is the distance from the surface at which collapse occurs. The radius of the bubbles decreases with increasing heat flux, but d_s increases as heat flux increases and the superheated layer thickens. Thus, the collapse intensity decreases as boiling becomes more intense.

In order to account for the effect of heat flux as well, a boiling parameter representing the evaporation rate is included. The removal/exchange constant accounting for the collapsing bubbles is then written:

$$k_{collapse} = \frac{q}{L} I \quad (17)$$

Under bulk boiling conditions, the temperature gradient is lower and the bubbles collapse far away from the heat transfer surface – if they collapse at all. The effect of the collapse is then much less and does not disturb the oxide deposit. The main cause for removal in this boiling regime is the detachment of bubbles at the nucleation sites; the turbulence created next to the bubble disturbs the top, labile portion of the deposit. As observed, only a certain part of

the deposit is subject to removal and we postulate that the bottom part is consolidated.

The effect of bubble detachment, k_{detach} , can be represented by the fraction of already deposited particles trapped by the bubble leaving the nucleation site. This is a function of the amount deposited at the previous nucleation. The particles trapped at the bubble surface, but which did not deposit, are not considered here. The removal constant for bulk boiling is then written as follows:

$$k_{detach} = \frac{\zeta}{\rho_p} \quad (18)$$

Finally, diffusion from the deposit to the bulk is a removal mechanism that is negligible under boiling conditions but is dominant for non-boiling heat transfer systems. The pertinent removal constant, k_{diff} , can be written as follows:

$$k_{diff} = a \frac{u^*}{Sc^{3/4}} \quad (19)$$

where a is an adjustment parameter equal to 0.8 under non-boiling conditions.

For bulk boiling where the collapsing effect is null, only the detachment of bubbles and diffusion will act. Under sub-cooled boiling, the collapse effect dominates. Under non-boiling conditions, only diffusion influences removal. The overall removal fluxes are written differently for each heat transfer regime.

- Non boiling : $\Phi_r = (C_b - C_s) k_{diff}$ (20)

- Sub-cooled boiling: $\Phi_r = k_{collapse} C_s$ (21)

- Bulk boiling: $\Phi_r = k_{detach} C_s$ (22)

In these equations, C_s is the concentration of iron oxide particles at the heat transfer surface.

Nucleation site stifling and consolidation

In the present model, nucleation sites are assumed to stifle after generating a certain amount of deposit and new ones are activated (as observed by McCrea (2001)). This stifling phenomenon, accompanied by site re-activation, is the reason for a complete deposit over the full surface of the heat transfer tube. The spots of deposit have a ring shape, the inside of which has a sparse covering of particles. We assume that an active nucleation site may stifle when the sparse deposit reaches a certain thickness. This occurs when a monolayer completely covers the inside of the ring. Such time can be calculated by computing the deposition flux in this region. Figure 2 shows this stifling mechanism.

It is assumed here that when a site stifles, a new site is activated in order to maintain the active nucleation site

density constant. We can then calculate the minimum time for complete coverage of the surface with deposit, which would be the time if there were no reactivation of stifled sites (Table 1).

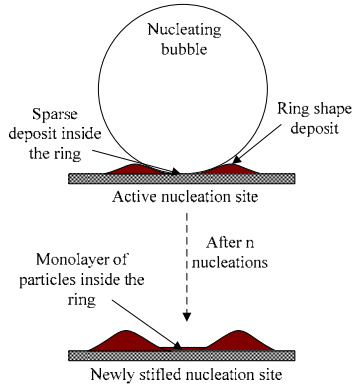


Fig. 2 Mechanism of stifling of a bubble nucleation site

Further in this section, it is shown that consolidation takes place under bulk boiling conditions from the start of the deposition and the consolidated portion can be calculated from a parameter that we define. In sub-cooled boiling, previous studies (Basset, 2000) led to the suggestion that all the deposit was labile and could be removed/ exchanged and that consolidation did not occur. However, the current model implies that consolidation also takes place in this boiling regime but only after a certain time, when some stifled sites get reactivated. The chimney effect is then dominant at that spot and, as the deposit builds up at the site, the bottom portion consolidates.

Now, if we consider a stifled nucleation site, we assume that such a site can be reactivated only when its next neighbours are also stifled. It is characterized here for simplicity by the time needed to cover the surface with at least a monolayer. The heat transfer surface is then under the influence of both the nucleation effect and the chimney effect for a transition period between sub-cooled or bulk boiling to wick boiling, when the chimney effect dominates.

Only a fraction of the deposited particles is consolidated and such a fraction varies with heat flux and bulk temperature. To account for it, we compute the quotient of the surface covered by active nucleation sites over the evaporation rate of bubbles, which is a measure of the boiling intensity. Then:

$$m_{labile} \propto \frac{A_{site} N_{active}}{q/L} \quad (23)$$

The consolidated deposit for sub-cooled boiling is now defined as follows:

$$m_{consolidation}(t) = m_{labile} a_c \left(\frac{t}{t_c} - 1 \right) \quad (24)$$

where t_c is the time when consolidation first occurs, and the constant a_c is equal to 10^{-4} . This equation is only valid for $t > t_c$.

The start time of the first spot to undergo consolidation is defined statistically by assuming that all the six (on average) closest neighbours of a stifled site must themselves become inactive before the first site can reactive. It has to be considered that the neighbours will not activate immediately after a site is stifled, so for fitting this model to the results of Basset (2000) we define t_c as follows:

$$t_c = 12 t_{stifle} \quad (25)$$

Before this critical time t_c , the consolidation term is equal to zero.

For bulk boiling, Cossaboom's (2005) results suggest that consolidation occurs from the start of deposition. Therefore a consolidation flux is included to account for it. The consolidated constant is also based on the labile parameter defined in Eq. (23) and is defined as:

$$k_c = (1 - m_{labile}) b_c \quad (26)$$

where b_c is a constant equal to 10^{-5} ; k_c operates on the total deposit (spikes from Cossaboom (2005) experiments are excluded).

General equations

To represent the amount deposited on the heat transfer surface, different approaches are used for the two different boiling regimes. A modified Kern and Seaton model is used for sub-cooled boiling and is written as follows:

$$m(t) = \frac{\Phi_d}{k_r} \left(1 - e^{-k_r t} \right) \quad (27)$$

where Φ_d is defined in equation (13) and k_r is defined as $k_{collapse}$ in equation (17). The consolidation term defined in equation (24) is added when the time is greater than the critical time defined in equation (25). For non-boiling systems, k_r is defined as k_{diff} in equation (19).

For bulk boiling, the consolidation model defined by Turner and Klimas is modified by the inclusion of our different fluxes defined earlier. The general equation for the amount of iron oxide deposited is written as follows:

$$m(t) = \frac{\Phi_d}{k_r + k_c} \left[k_c t + \frac{k_r}{k_r + k_c} \left(1 - e^{-(k_r + k_c)t} \right) \right] \quad (28)$$

where Φ_d is defined in equation (13), k_r is defined as k_{detach} in equation (18) and k_c is defined in equation (26).

For the radiotracing experiments, the release periods are modelled with a decreasing exponential function including the release/exchange and the consolidation constants.

EXPERIMENTS

In order to have a better understanding of the effect of bubbling on particle movement, visual studies have been undertaken using a high speed camera recording up to 500fps.

Bubbling tank

The first experiments were conducted using a 7L transparent cylindrical tank filled with a suspension of particles in which air bubbles were injected using nucleation holes at the bottom. Bubble frequency was changed as desired. Experiments using one hole and two adjacent holes were performed with the aim of revealing the hydrodynamic influences of bubbling on particle movement near nucleation sites. A total of forty runs were performed.

Two types of particles were used. The first were commercial resin, pliolites AC5G, with a size ranging from 1mm to few μm , and with a specific gravity close to one to maintain a good suspension in water at a concentration of 0.17 w/w%. The other particles were 50 μm -diameter glass balls; they had a much higher specific gravity and were uniformly deposited on the bottom of the tank.

High-speed movies were made of the pliolite suspension at the orifices for a range of bubbling frequencies and for one or two "active sites" (nucleation holes). Visual observations of the glass balls were made for similar variation of bubbling rate.

Recirculating loop

The second experiment was performed with a recirculating loop (Fig. 3) which can generate different modes of heating ranging from single phase convection to bulk boiling. Pure water was taken from a 180L tank using a centrifugal pump able to generate different flow rates and directed to enter the test section, a 1.5m-long and 9.93cm-diameter vertical glass column containing a 30 cm-long and 1.59 cm-diameter Alloy 800 steam generator tube polished to 600 sand paper grit. Inside this tube was a 25 cm-long heating cartridge capable of delivering a heat flux up to 240 kW/m^2 . The water temperature was pre-heated to about 90°C and the pressure in the test section was 136 kPa. The Reynolds number in the test section was maintained at about 8500.

The high-speed recording camera was focused on a small part of the heating tube and thirty movies of boiling behaviour were recorded for different heat fluxes. Bubble

size was measured and nucleation frequencies were calculated by using a frame-by-frame technique.

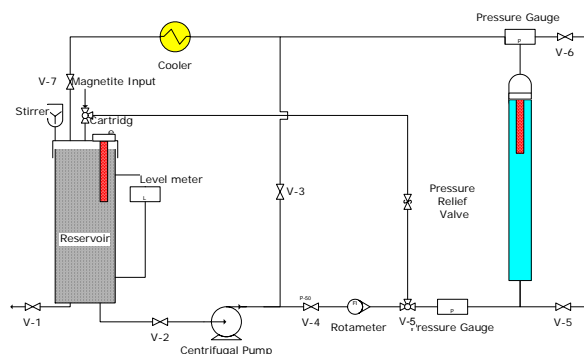


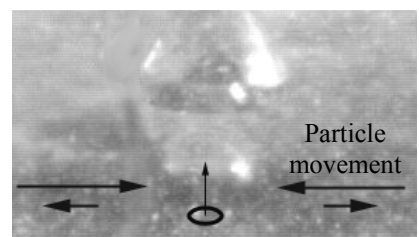
Fig. 3 Recirculating loop

RESULTS AND DISCUSSION

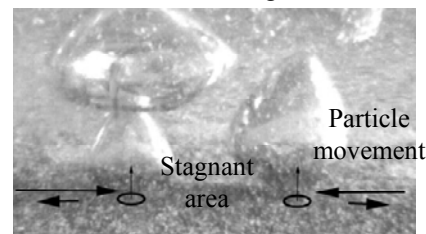
Bubbling tank results

The first experiment was to observe the influence of bubbles in a bubbling tank filled with particles.

Figure 4 shows pictures from high speed movies recorded with a suspension of pliolite particles. These movies showed a pumping effect (particles pushed away / attracted) that is represented on the picture by the arrows in the vicinity of the bubbling site in Fig. 4.a. For two bubbling sites, the situation was not so clear. As represented by Fig. 4.b, the pumping effect still occurred in the vicinity of the bubbling sites but between the two sites, the forces seemed to counteract each other, resulting in a stagnant zone.



a. One bubbling site



b. Two bubbling sites

Fig. 4 Pliolite suspension in the bubbling tank

Figure 5 shows the deposit morphology before and after bubbling with glass balls at the bottom of the bubbling tank. Figure 5.a shows a depleted area around the bubbling site. All the particles in this zone were attracted towards the bubbling site where the surface concentration was about twice as much as the average concentration everywhere else in the tank. With two bubbling sites (Fig. 5.b), the same phenomenon was observed as with the Pliolite suspension, with a relative stagnant area between the two sites.

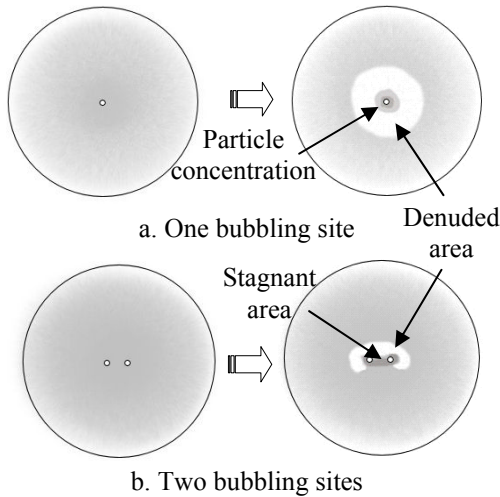


Fig. 5 Glass ball deposit in the bubbling tank

Recirculating loop results

Using the recirculating loop, bubble size and frequency as a function of heat flux under sub-cooled boiling conditions were recorded and are shown in Fig. 6 and Fig. 7 respectively.

The average bubble departure diameter decreases with increasing heat flux. This trend is in accordance with other data from Basset (2000). However, the present values are higher (about 5%), probably because Basset used a non-polished tube painted black for visual contrast, as opposed to the polished tube used here.

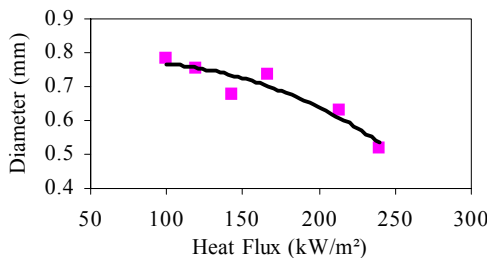


Fig. 6 Average bubble departure diameter vs. heat flux under sub-cooled boiling conditions

The bubble frequency increases with heat flux. It should be noted that bubble growth times were not affected by heat flux. However, the quantity of bubbles per unit surface area increased. Therefore, nucleation site density is also affected by a change in heat flux. Note that the total period between two bubbles is equal to the bubble growth time and the waiting time. Therefore, the increase of the bubble frequency with a constant bubble growth time implies a decrease in the waiting period.

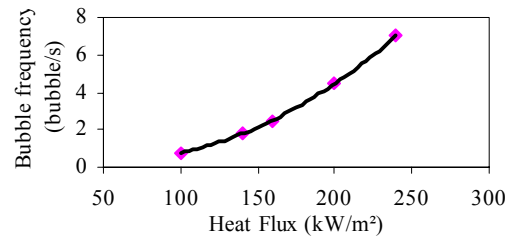


Fig. 7 Bubble frequency vs. heat flux under sub-cooled boiling conditions

Model predictions

Deposition under sub-cooled boiling conditions. The first set of predictions is for sub-cooled boiling. To obtain the predictions, the radius of each bubble was first computed for each heat flux during one nucleation, along with the quantities Φ_d , k_r , t_c and k_c . Then, once the fluxes for one nucleation were known, they were averaged over time and surface area. The complete model was then computed with time. Model predictions of the amount deposited after ten hours are shown in Fig. 8.

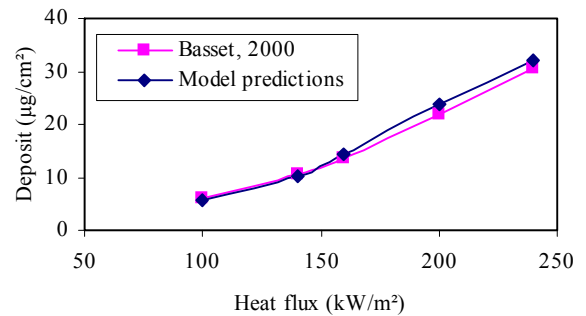


Fig. 8 Model predictions for the first 10 hours, [C]=5ppm

It can be observed that the model predictions are in good agreement with the experimental data. All predictions fit within 10% of Basset’s data. The amount deposited is mostly controlled by the number of particles trapped by the bubble. Although a pumping effect was observed during the

visualisation experiment, its relative importance compared to trapping turned out to be small (5% to 10%).

Model predictions of deposition as a function of time for different heat fluxes are given in Fig. 9. It can be seen from these curves that deposition rate decreases as time increases and as deposit thickens on the surface. Note that the deposit is in the form of small rings of diameter slightly smaller than the departure diameter of the bubbles. The inside of the ring is covered by a thin deposit. Filtration is the mechanism expanding the ring as it occurs from the sides and the top of the deposit. The time needed to stifle one site, i.e. fill the inside of a deposit ring with at least a monolayer of particles, is shown in Table 1. The best fit when plotting these values gives a covering time proportional to the power -2.6 of the heat flux. Note that at the predicted time when there is at least a monolayer everywhere on the unit surface, most of the deposit is in the form of spots or rings where the inside is filled more slowly. Thus, the average thickness of the deposit is about 8 to 9 times greater than one monolayer.

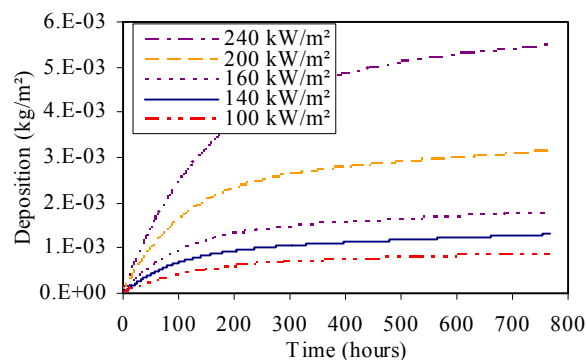


Fig. 9 Deposition at different heat fluxes vs. time ([C]=5ppm)

In the context of the assumption that sites get stifled and new ones are activated, the time needed to cover the whole surface with at least a monolayer is calculated at different heat fluxes; the results are shown in Table 1 along with the average reactivation time for nucleation sites. These reactivation times decrease as the heat fluxes increase, as would be expected, since deposition fluxes also increase.

Table 1. Stifling, covering and reactivation times at different heat fluxes ([C]=5ppm)

Heat Flux (kw/m ²)	100	140	160	200	240
Stifling time (hours)	4.6	3.7	3.3	3.0	2.9
Covering Time (hours)	750.9	283.9	197.4	110.0	74.8

Reactivation Time (hours)	55.32	44.18	39.37	35.88	34.43
---------------------------	-------	-------	-------	-------	-------

The curves in Fig. 9 tend to a linear increase showing a steady-state increase of the deposit. The consolidated portion can be considered as growing beneath the labile portion; in reality there will be lateral variations – particularly in the early stages as the spots or rings are forming. After a long time, the effect of microlayer evaporation compared to filtration becomes negligible. The water percolates in the capillaries of the deposit and releases vapour in the chimneys, emerging as bubbles. The transition between the regular boiling and this wick boiling regime occurs between about 100 and 500 hours, depending on the heat flux.

Deposition under bulk boiling conditions. Bulk boiling generally produces thicker deposits than sub-cooled boiling. Fig. 10 shows the comparison between models for the two boiling regimes under similar conditions. Deposition under bulk boiling is almost linear after 10 to 20h. The labile layer and the consolidated layer are both increasing linearly. The deposition rate is still falling for sub-cooled boiling after 400h.

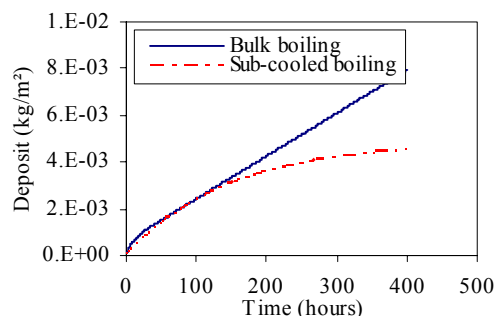


Fig. 10 Effect of time under different boiling regimes ([C]=5ppm)

Radiotracing experiments. The model has been applied to the experimental conditions of the previous radiotracing experiments. The first predictions are given for the experiment under sub-cooled boiling conditions. As stated before, Basset (2000) found good agreement with a first-order Kern and Seaton model. However, the new model incorporating consolidation fits rather better. Model predictions are shown in Fig. 11.

The consolidated portion accounts for about 20% of the total deposit at the beginning of the release period at 240h. In the final deposition period after ~ 400 h, the bulk concentration in the experiment increased, leading to the slight upward curve of the prediction.

For bulk boiling, the new model predictions have been compared to the experimental data from Cossaboom’s (2005) experiment and can be seen in Fig. 12. The irregular nature of the data in the first 20h or so of the experiment is attributed to unsteady bulk concentrations of activity. In particular, a spike in concentration occurred at valve-in time, leading to an apparent initial deposit at time 0h.

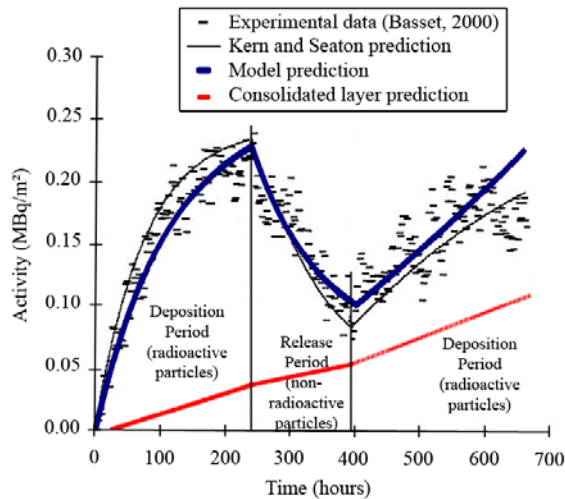


Fig. 11 Model predictions for radiotracing experiment under sub-cooled boiling conditions

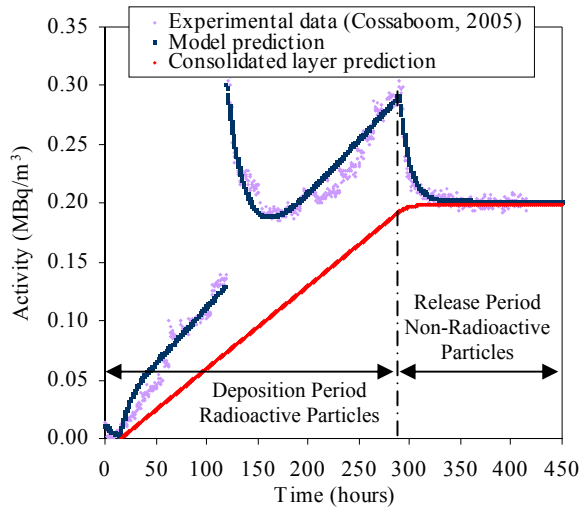


Fig. 12 Model predictions for radiotracing experiment under bulk boiling conditions

At $t = 120$ hours, a major spike in source concentration occurred during the experiment. As a result, a major burst in deposited activity occurred. The fact that the original trend of the data resumed after the spike indicates that the transient deposit was not consolidated. Note, however, the ~70% consolidation of the overall deposit indicated by the

release period after 290h. We interpret these observations as indicating a consolidated layer that builds up almost independently of the labile layer that undergoes release/exchange. The consolidated layer may well be at the metal-deposit interface, growing below the rings of deposit at the nucleation sites, as suggested earlier for sub-cooled boiling.

The release/exchange constant for the spike to give the model fit shown in Fig. 12 is $1.2 \times 10^{-5} \text{ s}^{-1}$ whereas the constant for the period after 290h is $2.9 \times 10^{-5} \text{ s}^{-1}$. The difference could reflect different behaviour of the transient “spike” deposit from that of the continuing labile deposit, though the values are close enough to derive from the same behaviour obscured by the scatter in the measurements.

The parameters obtained from fitting the models to the data for the two boiling regimes under similar operating conditions are presented in Table 2.

Table 2. Summary of the parameters for the two radiotracing experiments

	Sub-cooled boiling	Bulk boiling
Bulk temperature (K)	363	369
Heat Flux (kW/m^2)	190	240
Bubble frequency ($\text{s}^{-1}\text{site}^{-1}$)	4.4	7
Active nucleation site density (site/m^2)	8.07×10^4	1.64×10^5
Suspension concentration of radioactivity (MBq/m^3)	4.82	2.58
Deposition constant (m/s)	1.15×10^{-7}	5.28×10^{-6}
Removal constant (s^{-1})	2.70×10^{-6}	2.88×10^{-5}
Consolidation constant (s^{-1})	9.03×10^{-7}	6.86×10^{-6}
Consolidated portion of the deposit (%)	28.0	69.1
Stifling time (hours)	3	2.8
Start of consolidation (hours)	36	0
Covering time (hours)	115	31

CONCLUSIONS

To describe previous experimental results of particulate oxide deposition under sub-cooled and bulk boiling conditions, simple first-order deposition-release models are inadequate. Consolidation must be accounted for, and even then it must be recognized that rapid transients behave differently from steady accumulations – at least in bulk boiling.

Mechanistic models based on observations of boiling and of the interactions of nucleating bubbles with suspended particles are proposed. Microlayer evaporation, particle filtering through rings of deposit, particle trapping at the surface of growing bubbles and an increase in concentration at bubble nucleation sites by a pumping action as bubbles deposit are considered. The models fit the data of previous

deposition experiments quite well, describing the formation of rings or spots of deposit at bubble nucleation sites and suggesting how they develop into steam chimneys that support wick boiling as they thicken.

The labile or unconsolidated portion of the deposit is about 80% under sub-cooled boiling conditions and 30% under bulk boiling. The difference is probably due to the disturbances caused by bubble collapse in the former case, though the release/exchange constant of the labile layer is smaller for sub-cooled than for bulk boiling ($2.7 \times 10^{-6} \text{ s}^{-1}$ Vs 1.2 to $2.9 \times 10^{-5} \text{ s}^{-1}$).

ACKNOWLEDGEMENTS

The authors would like to thank the Natural Sciences and Engineering Research Council of Canada for financial support, and Ivan Kantor, Kittima Khumsa-Ang and Andrew Feicht for help in the laboratory.

NOMENCLATURE

A_{site}	surface area of a nucleation site, m^2
BR	boiling enhancement parameter, dimensionless
C_b	concentration in the bulk, kg/m^3
C_w	concentration at the wall, kg/m^3
d_s	distance of the bubble from the surface, m
f	bubble nucleation frequency, nucl/s
h	ring deposit thickness, m
I	turbulence intensity, %
k_c	consolidation constant, s^{-1}
k_{collapse}	removal constant due to collapsing bubbles, s^{-1}
k_{detach}	removal constant due to detaching bubbles, s^{-1}
k_{diff}	removal constant due to diffusion, s^{-1}
K	deposition rate coefficient, dimensionless
K_{diff}	diffusion coefficient, m/s
K_{th}	thermophoretic velocity, m/s
L	latent heat of vaporisation, J/kg
m	mass, kg
m_{labile}	labile parameter, dimensionless
m_{spot}	mass of a ring deposit, kg
N_{active}	active nucleation site density, $\text{NuclSite}/\text{m}^2$
q	heat flux, kW/m^2
R_b	bubble radius, m
Sc	Schmidt number, dimensionless
t	time, s
t_c	critical time for start of consolidation, s
t_{stifle}	time taken by a nucleation site to stifle, s
T_{film}	temperature of film, K
T_{sat}	saturation temperature, K
u*	friction velocity, m/s
V	flow velocity in the bulk, m/s
V_1, V_2, V_3	volumes defined in Figure 1, m^3
V_{filt}	volume of liquid filtered, m^3
V_t	volume of the "skin", m^3
δ_{max}	maximum microlayer thickness, m

ζ	particle trapping coefficient, dimensionless
λ	thermal conductivity, W/mK
v	kinematic velocity, m^2/s
Φ_{boil}	particle deposition flux due to boiling, $\text{kg}/\text{NuclSite.Nucl}$
Φ_d	particle deposition flux, $\text{kg}/\text{m}^2.\text{s}$
Φ_{diff}	deposition flux due to diffusion, $\text{kg}/\text{m}^2.\text{s}$
Φ_{filt}	deposition flux due to filtration, $\text{kg}/\text{NuclSite.Nucl}$
Φ_{nucl}	deposition flux due to bubble nucleation, $\text{kg}/\text{NuclSite.Nucl}$
Φ_{th}	deposition flux due to thermophoresis, $\text{kg}/\text{m}^2.\text{s}$
Φ_{wait}	deposition flux in period between bubbles, $\text{kg}/\text{NuclSite.Nucl}$
Φ_r	particle removal flux, $\text{kg}/\text{m}^2.\text{s}$
ρ	density, kg/m^3

Subscript

p	particle
v	vapour
w	water

REFERENCES

- Asakura, Y., Kikuchi, M., and Uchida, S., 1978, Deposition of Iron Oxide on Heated Surfaces in Boiling Water, *Nuclear Science and Engineering*, V.67, N.1, pp.1-7.
- Basset, M., McInerney, J., Arbeau, N., and Lister, D.H., 2000, The fouling of Alloy 800 heat exchange surfaces by magnetite particles, *The Canadian Journal of Chemical Engineering*, V.78, pp.40-52.
- Brennen, C.E., 1995, Cavitation and Bubble Dynamics, *Oxford University Press*.
- Cossaboom, J.L. and Lister, D.H., 2005, The Fouling of Alloy 800 Heat Exchanger Tubes by Nickel Ferrite Under Bulk Boiling Conditions, ECI Symposium Series, *Proc. 6th Int. Conf. Heat Exchanger Fouling and Cleaning*, Kloster Irsee, Germany, V.RP2, pp.109-118.
- Kern, D.Q. and Seaton, R.E., 1959, A Theoretical Analysis of Thermal Surface Fouling, *British Chemical Engineering*, V.4, pp.258-262.
- Levich, V.G., 1962, Physicochemical Hydrodynamics, *Prentice-Hall Inc*, New Jersey, USA.
- McCrea, L., 2001, Deposition of corrosion product particles onto heat exchange surfaces, *Master's Thesis*, University of New Brunswick.
- McNab, G.S. and Meisen, A, 1973, Thermophoresis in Liquids, *Journal of Colloid and Interface Science*, V.44, N.2, pp.339-346.
- Torigai, 1966, *Trans. Jpn. Soc. Mech. Eng.*, N°32, pp.1265.
- Turner, C. W. and Klimas, S. J., 2001, The Effect of Surface Chemistry on Particulate Fouling under Flow-Boiling Conditions, *Proc. Eng. Foundation Conf. Heat Exchanger Fouling*, Davos, Switzerland, pp.19-26.